A Search for Sterile Neutrinos at the NOνA Far Detector

A DISSERTATION PRESENTED
BY
GARETH KAFKA
TO
THE DEPARTMENT OF PHYSICS

IN PARTIAL FULFILLMENT OF THE REQUIREMENTS
FOR THE DEGREE OF
DOCTOR OF PHILOSOPHY
IN THE SUBJECT OF
PHYSICS

HARVARD UNIVERSITY
CAMBRIDGE, MASSACHUSETTS
MAY 2016

Thesis advisor: Professor Gary Feldman Gareth Kafka

A Search for Sterile Neutrinos at the NOνA Far Detector

Abstract

NOνA is the current United States flagship long-baseline neutrino experiment designed to study the properties of neutrino oscillations. It consists of two functionally identical detectors each located 14.6 mrad off the central axis from the Fermilab NuMI neutrino beam. The Near Detector is located 1 km downstream from the beam source, and the Far Detector is located 810 km away in Ash River, Minnesota. This long baseline, combined with the ability of the NuMI facility to switch between nearly pure neutrino and anti-neutrino beams, allows NOνA to make precision measurements of neutrino mixing angles, potentially determine the neutrino mass hierarchy, and begin searching for CP violating effects in the lepton sector. However, NOνA can also probe more exotic scenarios, such as oscillations between the known active neutrinos and new sterile species.

This thesis showcases the first search for sterile neutrinos in a $3 + 1$ model at NOνA. The analysis presented searches for a deficit in the rate of neutral current events at the Far Detector using the Near Detector to constrain the predicted spectrum. The comparison between the observed and predicted spectra is translated into a measurement of the expanded PMNS mixing matrix elements, $|U_{\mu 4}|^2$ and $|U_{\tau 4}|^2$, assuming a value of $\Delta m^2_{41} \sim O(1\text{ eV}^2)$. This analysis was performed using data taken between February 2014 and May 2015 corresponding to 3.52×10^{20} protons on target. The best fit values for the matrix elements were $|U_{\mu 4}|^2 = 0.xy \pm a.bc$ and $|U_{\tau 4}|^2 = 0.vw \pm d.ef$, consistent with the no sterile neutrino hypothesis. At the end of this thesis there is a short discussion of future sensitivity improvements using a larger dataset.

Contents

List of Figures

List of Tables

This is the dedication.

Acknowledgments

These people were cool.

1

A Brief History of Neutrinos

1.1 Introduction

The neutrino was first postulated by Wolfgang Pauli as a possible explanation for the continuous spectrum of electrons emitted from nuclear β decay [1]. This decay was originally thought to be the emission of an electron from an atom, resulting in a different nucleus, via the process,

$$N \rightarrow N' + e \tag{1.1}$$

where N and N' are the parent and daughter nuclei, respectively. In a two body decay such as this, the momenta and energies of the outgoing particles are exactly constrained. Pauli's new particle explained the continuous spectrum of electron energy via a modified decay process:

$$N \rightarrow N' + e + \nu \tag{1.2}$$

where ν is the outgoing neutral particle. Pauli's original proposal called the new particle the neutron, but this name was later used to name the massive neutral nucleon discovered by Chadwick in 1932 [2]. Three years after Pauli's idea, Fermi proposed a model for nuclear β decay that included the new particle, which he coined the neutrino, or little neutral one [3].

1.2 First Detection of Neutrinos

Twenty years passed from Fermi's model proposal before neutrinos were discovered experimentally. Fred Reines and Clyde Cowan made the discovery by placing a detector near a nuclear reactor as a source of neutrinos and observing inverse β decay [4, 5]. The neutrinos observed were anti-electron neutrinos, thus the following was the observed process.

$$p + \bar{\nu}_e \rightarrow n + e^+ \tag{1.3}$$

Reines earned the Nobel Prize in Physics in 1995 for the detection of the neutrino.

In 1962, the muon neutrino was discovered at Brookhaven National Laboratory using the first neutrino beam [6] in a scheme still used in neutrino experiments today. The beam was generated by colliding protons with a target, producing pions that decayed into muons and muon neutrinos. The resultant beam then passed through thick steel, absorbing everything but the neutrinos. Leon Lederman, Melvin Schwartz, and Jack Steinberger won the Nobel Prize in Physics in 1988 for the discovery of the muon neutrino.

The last generation of neutrino, the tau neutrino, was discovered at Fermilab by the DONUT collaboration in 2000 [7].

1.3 Evidence of Neutrino Oscillations

Pontecorvo first postulated neutrino oscillations between neutrinos and anti-neutrinos, analogous to $K^0/\bar{K}^0$ oscillations, in 1957 [8]. Nothing came of the proposal immediately, but the idea was later revived and modified to solve the solar neutrino problem. The physics community initially viewed neutrino oscillations with skepticism and believed the experiments to be flawed, but over time oscillations have become an unmistakable and accepted phenomenon.

The solar neutrino problem was born from a large discrepancy between the theoretical and observed number of neutrinos produced by the sun. Neutrinos were used as a study for solar models because photons take a thousand years to escape the dense nuclear plasma to the surface of the sun, but neutrinos are unimpeded. The models, which have been confirmed today, describe a somewhat complicated chain of nuclear reactions, many of which produce neutrinos. Each individual process contributes a neutrinos in a different energy spectrum, but all of the neutrinos are created as electron neutrinos.

The experimental observations and theoretical predictions were both published in 1968. Ray Davis designed an experiment underground in the South Dakota Homestake mine consisting of a tank of an ultra pure chlorine cleaning solution capable of neutrino capture via the process

$$\nu_e + {}^{37}\mathrm{Cl} \rightarrow {}^{37}\mathrm{Ar} + e^- \tag{1.4}$$

The argon atoms could be collected and counted for a direct measurement of the neutrino flux [9]. Meanwhile, John Bahcall precisely calculated the expected neutrino flux [10], and the observed rate was found to be about one third of the predicted rate. Pontecorvo revived his theory with the modification of allowing ν_e to ν_μ oscillations [11], but the idea was still not taken seriously and it was another 20 years before the solar neutrino problem was confirmed.

Beginning in 1989, multiple experiments with different methodologies confirmed the solar neutrino problem. Kamiokande, a water Cherenkov detector, measured a rate deficit in 1989 [12]. Two experiments measured solar neutrinos via the reaction

$$\nu_e + {}^{71}\mathrm{Ga} \rightarrow {}^{71}\mathrm{Ge} + e^- \tag{1.5}$$

and measured a similar deficit, SAGE in 1991 [13] and GALLEX in 1992 [14]. With results from three different experimental methods all showing similar rate deficits, the solar neutrino problem could no longer be relegated to an experimental error.

Evidence soon emerged for oscillations with atmospheric neutrinos as well. These neutrinos are produced when cosmic rays collide with particles in the atmosphere and decay, predominantly via the following channels.

$$
\begin{aligned}
\pi^{+/-} &\rightarrow \mu^{+/-} + \nu_\mu/\bar{\nu}_\mu \\
\mu^{+/-} &\rightarrow e^{+/-} + \nu_e/\bar{\nu}_e + \bar{\nu}_\mu/\nu_\mu
\end{aligned} \tag{1.6}
$$

Thus, the expected ratio of muon family neutrinos to muon family neutrinos was expected to be 2. Kamiokande measured this ratio in 1992 and found the ratio to be much closer to 1 [15]. Furthermore, the ratio seemed to be dependent on zenith angle, with the measurement being nearly 2 for neutrinos coming from directly overhead, and dropping as the angle increased. Super-Kamiokande (or Super-K), the successor to Kamiokande, improved upon this measurement in 1998 [16], providing the most definitive evidence of neutrino oscillations to that point.

A resolution to the solar neutrino problem did not have to wait much longer with detector technologies capable of discerning different neutrino interaction types. SNO was designed as a heavy water (D_2O) Cherenkov detector experiment to be sensitive to both the flux of electron neutrinos and the flux of all neutrinos. In 2002, it released results for these measurements, finding what was then the expected deficit in electron neutrino flux, but a total flux consistent with the standard solar model, see Fig. 1.1 [17]. With this result, neutrino oscillations were confirmed, and subsequent experiments now measure oscillation parameters with precision.

1.4 Possible Evidence of Sterile Neutrinos

There exists some evidence of more than three neutrinos, but the number of active neutrinos is constrained by measurements of the width of the Z boson. LEP has measured the number of active neutrinos to be 2.984 ± 0.008 [18], so the discoveries of the ν_e, ν_μ, and ν_τ leave no room for new active neutrinos. (Strictly speaking, there could be other active neutrinos if they had mass greater than half the mass of the Z boson so the Z could not decay to them, but the evidence that does exist suggests a mass

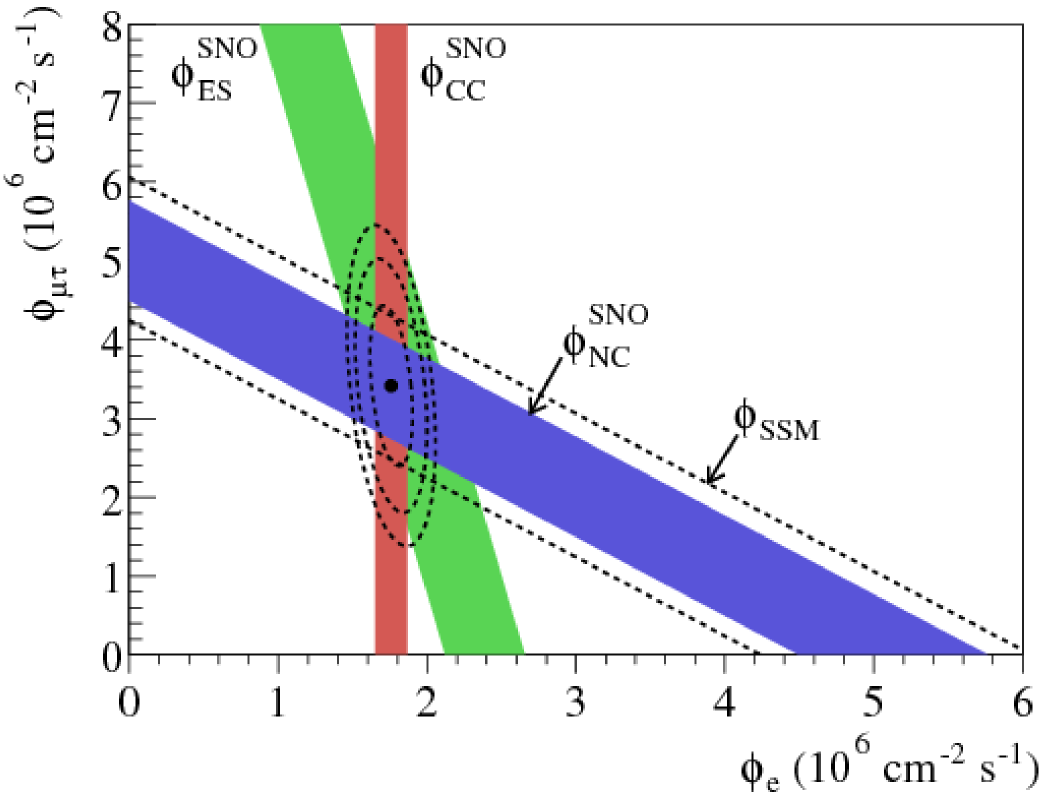

Figure 1.1: The measurement of different event rates at SNO [17]. The red band represents ν_e CC interactions with the deuterium neutron, an interaction only sensitive to electron neutrinos. The blue band represents neutral current scattering off of the deuterium nucleus, an interaction sensitive to the total neutrino flux. The green band represents elastic scattering of the neutrino off the deuterium electron, an interaction sensitive to all neutrino flavors, but not completely independent of neutrino flavor. The dashed straight lines represent the flux prediction by the standard solar model. The point represents the best fit for the flux of electron neutrinos and the flux for the combined muon and tau neutrinos.

splitting from the other neutrino states much smaller than this.)

The first evidence for an additional neutrino came from the Liquid Scintillator Neutrino Detector, or LSND, in 1995. This experiment searched for $\bar{\nu}_e$ appearance in a $\bar{\nu}_\mu$ beam. When it found an excess of events, it reported a measurement of a mass splitting between neutrino states Δm^2 of $O(1\ \text{eV}^2)$ [19]. The mass splitting affects the frequency of neutrino oscillations, and will be explained in greater depth in chapter 2. The measurement from LSND is incompatible with the mass splittings measured in both the atmospheric and solar oscillation experiments, suggesting the addition of at least one more neutrino. However, based on the result from LEP, this new neutrino can not couple to the Z boson, hence the suggestion for a sterile neutrino.

Many other experiments have tried to search for the existence of sterile neutrinos. The MiniBooNE experiment at Fermilab searched for both ν_e appearance in a ν_μ beam and $\bar{\nu}_e$ appearance in an $\bar{\nu}_\mu$ beam. While they first reported no event excess in 2007 [20], their more results show excesses in both modes [21] that could be consistent with some sterile neutrino models. Not all experiments have found evidence of sterile neutrinos, however. The most recent results from KARMEN in 2002 [22] and NOMAD in 2003 [23] showed no evidence of oscillations at the same mass scale as LSND. This list experimental evidence (or lack thereof) is by no means exhaustive, but it should be clear that there is not yet a scientific consensus on the existence of sterile neutrinos.

Today, most neutrino experiments have some form of analysis searching for a sterile neutrinos. The theory that would govern sterile oscillations (discussed in detail in section 2.6) is well understood, so individual experiments can try to measure or set limits on the various parameters introduced by adding sterile neutrinos to our current models. Recent measurements have come from an atmospheric neutrino measurement by Super-K in 2015 [24], a reactor experiment analysis by Daya Bay in 2014 [25], a short baseline detector analysis at the T2K near detector in 2015 [26], and a long baseline detector analysis by MINOS in 2011 [27].

NOνA is a long baseline neutrino experiment with a near detector, thus capable of performing both short baseline and long baseline sterile neutrino analyses; this thesis focuses on the long baseline. The analysis performed searches for a deficit in the number of neutral current events at the far detector, using the near detector data to constrain the predicted spectrum. Neutral currents are insensitive to the flavors of the standard 3 active neutrinos, so a rate deficit would point to the existence of a sterile neutrino.

2

Theory of Neutrino Oscillations

The idea of neutrino oscillations was first proposed by Pontecorvo in 1957 [8], but his proposal described oscillations between neutrinos and anti-neutrinos. In 1962, after the discovery of the muon neutrino, Maki, Nakagawa, and Sakata proposed the theory that described oscillations between neutrino flavors due to differing neutrino flavor and mass eigenstates [28]. This chapter describes the modern formalism in detail and uses natural units where $\hbar = c = 1$, except where otherwise noted.

2.1 The PMNS Matrix

In the Standard Model, neutrinos only interact via the W and Z bosons as shown by the Feynman diagrams in Fig. 2.1. From these diagrams, it is clear that neutrinos always interact in a definite flavor eigenstate, $|\nu_\alpha\rangle$. Furthermore, when a neutrino is produced from a W boson, the flavor is always determined

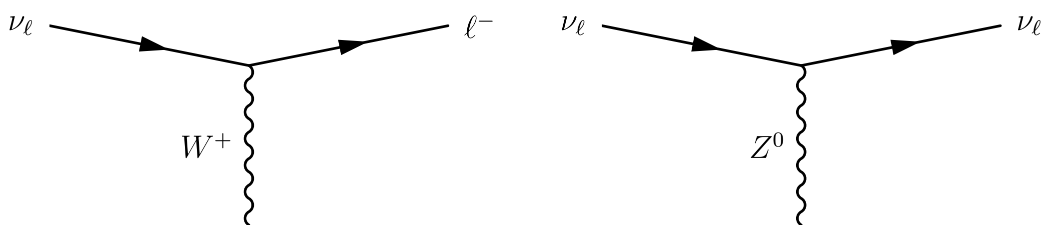

Figure 2.1: Standard Model Weak interactions involving a neutrino. Left: Charged current interaction. Right: Neutral current interaction.

by the associated charged lepton shown in eq. 2.1.

$$\begin{pmatrix} \nu_e \\ e \end{pmatrix}, \quad \begin{pmatrix} \nu_\mu \\ \mu \end{pmatrix}, \quad \begin{pmatrix} \nu_\tau \\ \tau \end{pmatrix} \tag{2.1}$$

On the other hand, neutrinos propagate through spacetime with a definite mass, $|\nu_i\rangle$ an eigenstate of the free Hamiltonian. The flavor states can be written as a superposition of the mass states via

$$|\nu_\alpha\rangle = \sum_{i=1}^{n} U^*_{\alpha i} |\nu_i\rangle , \tag{2.2}$$

where n is the number of neutrinos, and U is the unitary PMNS matrix, named after Pontecorvo, Maki, Nakagawa, and Sakata. The PMNS matrix is unitary, and would reduce to the identity matrix if neutrinos did not oscillate between flavor states. Yet since it does provide the mechanism for flavor transitions, it can be thought of as analogous to the quark sector CKM matrix.

2.2 Vacuum Oscillations

In this section, the basics of neutrino oscillations are developed by considering oscillations in a vacuum. The neutrinos are treated as plane waves, as in [29], with the assumption that the neutrino is actually localized in space put in by hand. A careful, rigorous analysis treating the neutrinos as plane waves in [30] reproduces the same results.

Consider a neutrino in a state of definite flavor α at time $t = 0$, $|\nu(0)\rangle = |\nu_\alpha\rangle$. This state is in a superposition of mass eigenstates. The time evolution of this neutrino is simply the time evolution of the individual mass states. In a vacuum, this adds a phase factor to each mass state.

$$|\nu_\alpha(t)\rangle = \sum_i U^*_{\alpha i} e^{-i(E_i t - \mathbf{p_i}\cdot\mathbf{x})} |\nu_i\rangle \tag{2.3}$$

With the neutrino at position $\mathbf{x} = L$ at time t, the dot product evaluates to $\mathbf{p_i}\cdot\mathbf{x} = p_i L$. Eq 2.3 can then simplified by making use of the fact that neutrinos are ultra-relativistic, allowing for several assumptions. First, the time, t, is replaced by the distance, L. Next, the energy of each mass state is approximated to be the same energy, $E_i = E$. Last, the momentum is expanded as $p_i = \sqrt{E^2 - m_i^2} \approx E - m_i^2/2E$. With these assumptions, eq. 2.3 simplifies as:

$$|\nu_\alpha(L)\rangle = \sum_i U^*_{\alpha i} e^{-im_i^2 L/2E} |\nu_i\rangle \,. \tag{2.4}$$

The mass eigenstate inside the sum is then re-expressed in terms of flavor eigenstates using the inverse of eq. 2.2 and unitarity of U.

$$|\nu_\alpha(L)\rangle = \sum_{\alpha'} \sum_i U^*_{\alpha i} U_{\alpha' i} e^{-im_i^2 L/2E} |\nu'_\alpha\rangle \,. \tag{2.5}$$

Eq. 2.5 can then be used to find the probability that the original neutrino in flavor state α has transitioned (or survived) as flavor state β. First, the matrix element $\langle\nu_\beta|\nu_\alpha(L)\rangle$ is computed.

$$\langle\nu_\beta|\nu_\alpha(L)\rangle = \sum_{\alpha'} \sum_i U^*_{\alpha i} U_{\alpha' i} e^{-im_i^2 L/2E} \langle\nu_\beta|\nu'_\alpha\rangle = \sum_i U^*_{\alpha i} U_{\beta i} e^{-im_i^2 L/2E} \tag{2.6}$$

The last equality in eq. 2.6 follows from the orthogonality of individual flavor eigenstates. The probability of the flavor transition is then the square of this matrix element.

$$P(\nu_\alpha \to \nu_\beta) = |\langle \nu_\beta | \nu_\alpha(L) \rangle|^2 = \sum_{i,j} U^*_{\alpha i} U_{\beta i} U^*_{\beta j} U_{\alpha j} e^{-i(m_i^2 - m_j^2)L/2E} \tag{2.7}$$

It is standard to rewrite the mass squared difference as $\Delta m^2_{ij} \equiv m_i^2 - m_j^2$. Eq. 2.7 is then manipulated using the properties of unitary matrices.

$$\begin{aligned} P(\nu_\alpha \to \nu_\beta) &= \sum_{i,j} U^*_{\alpha i} U_{\beta i} U^*_{\beta j} U_{\alpha j} + \sum_{i,j} U^*_{\alpha i} U_{\beta i} U^*_{\beta j} U_{\alpha j} (e^{-i\Delta m^2_{ij} L/2E} - 1) \\ &= \delta_{\alpha\beta} + \sum_{i,j} U^*_{\alpha i} U_{\beta i} U^*_{\beta j} U_{\alpha j} (e^{-i\Delta m^2_{ij} L/2E} - 1) \end{aligned} \tag{2.8}$$

The remaining summed term is further simplified making use of two facts. When $i = j$, the complex phase is 0 as $\Delta m^2_{ii} = 0$, and thus these terms vanish. Second, the terms with $i < j$ are complex conjugates of those with $i > j$, and $z + z^* = 2\Re(z)$ for any complex number z.

$$P(\nu_\alpha \to \nu_\beta) = \delta_{\alpha\beta} + 2\sum_{i>j} \Re\left[U^*_{\alpha i} U_{\beta i} U^*_{\beta j} U_{\alpha j} (e^{-i\Delta m^2_{ij} L/2E} - 1)\right] \tag{2.9}$$

Both pieces of this term are split into their real and imaginary parts, and simplified using the trigonometric identity $\cos 2\theta - 1 = -2\sin^2\theta$. Defining $\mathcal{U} \equiv U^*_{\alpha i} U_{\beta i} U^*_{\beta j} U_{\alpha j} (e^{-i\Delta m^2_{ij} L/2E} - 1)$ and $\phi \equiv \Delta m^2_{ij} L/2E$:

$$\begin{aligned} \Re(\mathcal{U}) &= \Re\left[U^*_{\alpha i} U_{\beta i} U^*_{\beta j} U_{\alpha j} (e^{-i\Delta m^2_{ij} L/2E} - 1)\right] & (2.10) \\ &= \Re\left\{\left[\Re(U^*_{\alpha i} U_{\beta i} U^*_{\beta j} U_{\alpha j}) + i\Im(U^*_{\alpha i} U_{\beta i} U^*_{\beta j} U_{\alpha j})\right]\left[-2\sin^2(\phi/2) - i\sin\phi\right]\right\} & (2.11) \\ &= -2\Re(U^*_{\alpha i} U_{\beta i} U^*_{\beta j} U_{\alpha j})\sin^2(\phi/2) + \Im(U^*_{\alpha i} U_{\beta i} U^*_{\beta j} U_{\alpha j})\sin\phi & (2.12) \end{aligned}$$

Inserting the expression from eq. 2.12 into eq. 2.9, we find:

$$\begin{aligned} P(\nu_\alpha \to \nu_\beta) = \delta_{\alpha\beta} \quad &- \quad 4\sum_{i>j} \Re(U^*_{\alpha i} U_{\beta i} U^*_{\beta j} U_{\alpha j}) \sin^2 \Delta_{ij} \\ &+ \quad 2\sum_{i>j} \Im(U^*_{\alpha i} U_{\beta i} U^*_{\beta j} U_{\alpha j}) \sin 2\Delta_{ij}, \end{aligned} \tag{2.13}$$

where $\Delta_{ij} \equiv \Delta m^2_{ij} L/4E = 1.267 \Delta m^2_{ij} L\,(\text{km})/E\,(\text{GeV})$. It can now be seen that the distance the neutrino travels, its energy, and the different mass splittings all affect the frequency of oscillation. Ideally, neutrino oscillations would be studied by having neutrinos with a fixed energy profile (preferably monoenergetic) and varying the baseline. However, neutrino detectors are incredibly large, so in practice the baseline is fixed and the oscillation probability is studied as a function of neutrino energy.

For the case of survival probability, $\alpha = \beta$ and eq. 2.13 simplifies further. The imaginary piece from eq. 2.13 drops out, as

$$\Im(U^*_{\alpha i} U_{\alpha i} U^*_{\alpha j} U_{\alpha j}) = \Im(|U_{\alpha i}|^2 |U_{\alpha j}|^2) = 0. \tag{2.14}$$

The survival probability is then given by:

$$P(\nu_\alpha \to \nu_\alpha) = 1 - 4\sum_{i>j} |U_{\alpha i}|^2 |U_{\alpha j}|^2 \sin^2 \Delta_{ij}. \tag{2.15}$$

Due to the combined influence of mass splitting, oscillation baseline, and neutrino energy on the oscillation probability, it is often the case that only one term contributes to the sums in eq.s 2.13 and 2.15. The two neutrino approximation can be instructive in this instance. For this model, the mixing matrix simplifies to the two dimensional rotation matrix:

$$U = \begin{pmatrix} \cos\theta & \sin\theta \\ -\sin\theta & \cos\theta \end{pmatrix}. \tag{2.16}$$

As this matrix is entirely real, the imaginary piece of eq. 2.13 drops out. Plugging the matrix elements into the remaining term directly and simplifying slightly, we find the following forms for the survival and appearance probabilities.

$$P(\nu_\alpha \rightarrow \nu_\alpha) \quad = \quad 1 - \sin^2 2\theta \sin^2\left(\frac{\Delta m^2 L}{4E}\right) \tag{2.17}$$

$$P(\nu_\alpha \nrightarrow \nu_\alpha) \quad = \quad \sin^2 2\theta \sin^2\left(\frac{\Delta m^2 L}{4E}\right) \tag{2.18}$$

From these equations it is clear that the mixing matrix parameters control the amplitude of neutrino oscillations. For small angles, most neutrinos will not change flavor, while larger angles can cause most of the neutrinos to change flavor. The case where $\theta = 45°$ is called maximal mixing as at specific baseline lengths the probability of oscillation becomes 1.

2.3 Standard 3-Flavor Oscillations

The Standard Model includes three neutrinos, so the PMNS matrix is 3×3 in this picture. Explicitly expanding eq. 2.2, U takes the following form:

$$\begin{pmatrix} \nu_e \\ \nu_\mu \\ \nu_\tau \end{pmatrix} = \begin{pmatrix} U_{e1} & U_{e2} & U_{e3} \\ U_{\mu 1} & U_{\mu 2} & U_{\mu 3} \\ U_{\tau 1} & U_{\tau 2} & U_{\tau 3} \end{pmatrix} \begin{pmatrix} \nu_1 \\ \nu_2 \\ \nu_3 \end{pmatrix}. \tag{2.19}$$

The PMNS matrix can be parametrized in terms of 3 real mixing angles, θ_{ij} and a complex phase, δ, called the CP phase. Following the convention from the Particle Data Group [31], the expanded matrix takes the form

$$\begin{aligned} U \quad &= \quad \begin{bmatrix} c_{12}c_{13} & s_{12}c_{13} & s_{13}e^{-i\delta} \\ -s_{12}c_{23} - c_{12}s_{23}s_{13}e^{i\delta} & c_{12}c_{23} - s_{12}s_{23}s_{13}e^{i\delta} & s_{23}c_{13} \\ s_{12}s_{23} - c_{12}c_{23}s_{13}s^{i\delta} & -c_{12}s_{23} - s_{12}c_{23}s_{13}e^{i\delta} & c_{23}c_{13} \end{bmatrix} \\ &= \quad \begin{bmatrix} 1 & 0 & 0 \\ 0 & c_{23} & s_{23} \\ 0 & -s_{23} & c_{23} \end{bmatrix} \begin{bmatrix} c_{13} & 0 & s_{13}e^{-i\delta} \\ 0 & 1 & 0 \\ -s_{13}e^{i\delta} & 0 & c_{13} \end{bmatrix} \begin{bmatrix} c_{12} & s_{12} & 0 \\ -s_{12} & c_{12} & 0 \\ 0 & 0 & 1 \end{bmatrix} \end{aligned} \tag{2.20}$$

where $c_{ij} \equiv \cos\theta_{ij}$ and $s_{ij} \equiv \sin\theta_{ij}$.

With three neutrinos, the expanded forms of eq.s 2.13 and 2.15 can still balloon into unwieldy messes. Fortunately, based on current knowledge of the mass splittings, it is usually the case that only one mass splitting scale matters and other terms can be dropped. Fig. 2.2 shows a schematic of the mass splittings. For historic reasons, Δm^2_{21} is known as the solar mass splitting and the larger mass splitting is called the atmospheric mass splitting. The atmospheric mass splitting is about 30 times the solar mass splitting. The sign of the solar mass splitting is known, while that of the atmospheric mass splitting is not. A positive value of Δm^2_{32} is called the normal hierarchy; a negative value is called the inverted hierarchy.

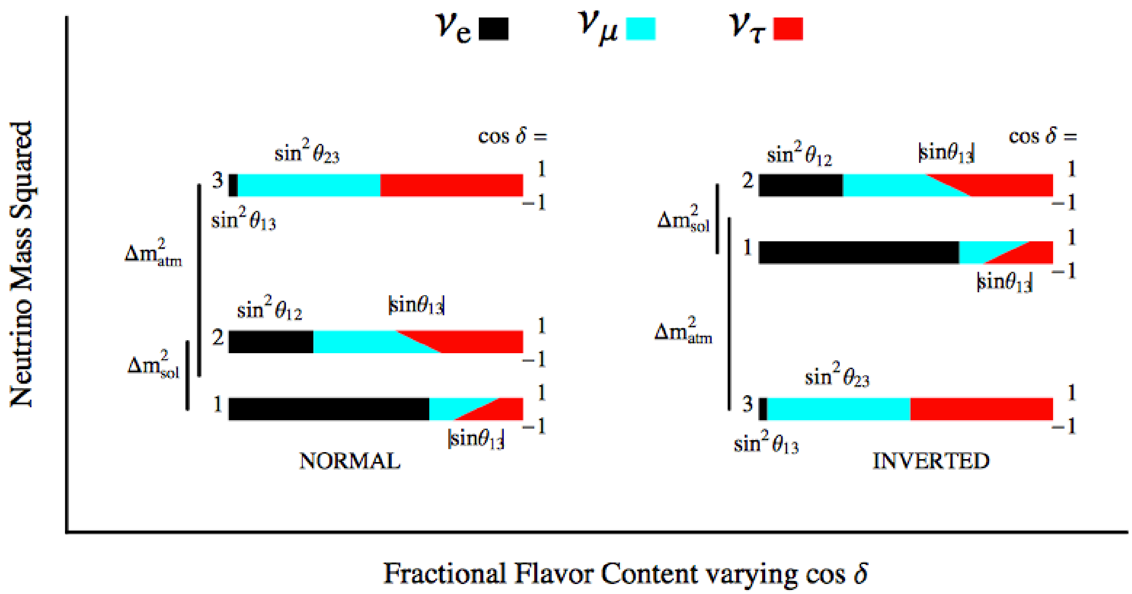

Figure 2.2: A schematic of the mass splittings between the three known neutrino mass states and how much they couple to each of the flavor states [32].

Two oscillation probabilities that are of interest to NOνA are the muon neutrino survival probability and electron neutrino appearance from a muon neutrino beam. Since $|\Delta m^2_{21}|$ is so much smaller than $|\Delta m^2_{32}|$, the solar oscillation baseline is much longer, thus the oscillation probability is first dominated by terms containing Δm^2_{32}. This is the case for NOνA. Furthermore, the probability can be simplified by making making the assumption that $|\Delta m^2_{32}| \approx |\Delta m^2_{31}|$. Under these conditions, the survival probability of muon neutrinos is calculated as follows:

$$
\begin{aligned}
P(\nu_\mu \to \nu_\mu) &\approx 1 - 4|U_{\mu 3}|^2(|U_{\mu 1}|^2 + |U_{\mu 2}|^2)\sin^2\Delta_{32} && (2.21)\\
&\approx 1 - 4s_{23}^2(1 - s_{13}^2)(c_{23}^2 + s_{23}^2 s_{13}^2)\sin^2\Delta_{32} && (2.22)\\
&\approx 1 - 4s_{23}^2 c_{23}^2 \sin^2\Delta_{32} + 4s_{23}^2 s_{13}^2(c_{23}^2 - s_{23}^2)\sin^2\Delta_{32} && (2.23)\\
&= 1 - \sin^2 2\theta_{23}\sin^2\Delta_{32} + 4\sin^2\theta_{23}\sin^2\theta_{13}\cos^2 2\theta_{23}\sin^2\Delta_{32} && (2.24)
\end{aligned}
$$

Between eq.s 2.22 and 2.23, the term proportional to s_{13}^4 was dropped using the current knowledge that s_{13}^2 is small [31]. Note that if θ_{13} were 0, then eq. 2.24 would reduce to eq. 2.17, the two neutrino survival probability.

The full 3 flavor electron neutrino appearance from muon neutrino oscillation probability is often written in the form [33]:

$$
P(\overset{(-)}{\nu}_\mu \to \overset{(-)}{\nu}_e) = P_{atm} + 2\sqrt{P_{atm}}\sqrt{P_{sol}}\left(\cos\delta\cos\Delta_{32} \overset{(+)}{-} \sin\delta\sin\Delta_{32}\right) + P_{sol} \qquad (2.25)
$$

where

$$
\begin{aligned}
\sqrt{P_{atm}} &\equiv \sin\theta_{23}\sin 2\theta_{13}\sin\Delta_{32} && (2.26)\\
\sqrt{P_{sol}} &\equiv \cos\theta_{23}\sin 2\theta_{12}\sin\Delta_{21} && (2.27)
\end{aligned}
$$

where the approximation $|\Delta m_{32}^2| \approx |\Delta m_{31}^2|$ has been made and higher order terms of s_{13}^2 been dropped. For an experiment at a short enough baseline such as NOνA, the P_{sol} term is negligible as it depends on a higher order term of the solar mass splitting. The cross term is also not the dominant effect as it also depends upon the solar mass splitting, but it demonstrates interesting behavior. The $\cos\delta$ term is CP conserving, but the $\sin\delta$ term exhibits CP violation. This is why δ is called the CP violating phase angle.

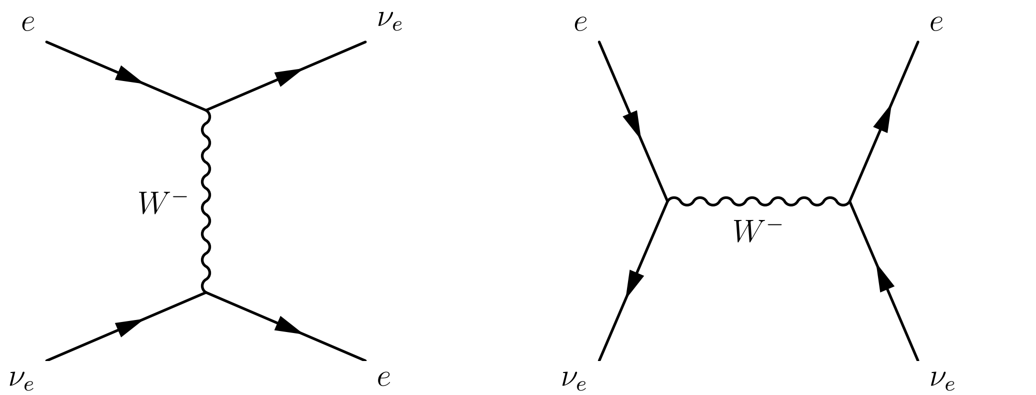

Figure 2.3: Coherent forward scattering interactions involved in the MSW effect. Left: Scattering of electron neutrinos on electrons. Right: Scattering of anti-electron neutrinos on electrons.

2.4 Matter Effects

So far, the oscillation formalism has been developed only considering neutrinos in a vacuum. However, most neutrino oscillation experiments involve neutrinos traveling through matter, be it the Sun or the Earth. This affects the oscillation probabilities in a process called the Mikheyev-Smirnov-Wolfenstein effect, or MSW effect. The phenomenon was first proposed by Wolfenstein in 1978 [34]; Mikheyev and Smirnov built upon that work in 1985 [35] as a possible solution for the solar neutrino problem.

The MSW effect is the coherent forward scattering of neutrinos off of the electrons in ordinary matter, a channel only available to electron flavor neutrinos and anti-neutrinos. Fig. 2.3 illustrates the interactions. The electrons contribute an additional potential term, $V_e = \pm\sqrt{2}G_F N_e$, where G_F is Fermi's constant, N_e is the electron number density, the positive sign is for neutrinos, and the negative for anti-neutrinos. Neutrinos also forward scatter off the neutrons and protons in matter via neutral current interactions, but this only provides an overall phase as all neutrino flavors participate in these interactions equally. The matter induced potential adds an additional term to the Schrödinger equation, affecting the time evolution of the flavor states and thus changing the oscillation probabilities.

The following derivation will consider the MSW effect in the case of two neutrino flavors. The time evolution of the flavor states is written as follows:

$$i\begin{pmatrix}\nu_e\\ \nu_\mu\end{pmatrix} = \left[U\begin{pmatrix}\frac{m_1^2}{2E} & 0\\ 0 & \frac{m_2^2}{2E}\end{pmatrix}U^\dagger + \begin{pmatrix}\pm V_e & 0\\ 0 & 0\end{pmatrix}\right]\begin{pmatrix}\nu_e\\ \nu_\mu\end{pmatrix} \tag{2.28}$$

Inserting the 2 flavor PMNS matrix from eq. 2.16, applying some trigonometric identites, and dropping common diagonal terms, eq. 2.28 simplifies to

$$i\begin{pmatrix}\nu_e\\ \nu_\mu\end{pmatrix} = \frac{1}{4E}\begin{pmatrix}-\Delta m_{21}^2\cos 2\theta \pm 4EV_e & \Delta m_{21}^2 \sin 2\theta\\ \Delta m_{21}^2\sin 2\theta & \Delta m_{21}^2\cos 2\theta\end{pmatrix}\begin{pmatrix}\nu_e\\ \nu_\mu\end{pmatrix}. \tag{2.29}$$

The diagonal terms are dropped because they can be absorbed by the phase convention of the neutrino states. This Hamiltonian can be re-diagonalized with another unitary transformation, $H_M = U_M^\dagger H U_M$, with the following results:

$$H_M = \frac{1}{2}\begin{pmatrix}-\frac{\Delta m_M^2}{2E} & 0\\ 0 & \frac{\Delta m_M^2}{2E}\end{pmatrix} \tag{2.30}$$

$$U_M = \begin{pmatrix}\cos\theta_M & \sin\theta_M\\ -\sin\theta_M & \cos\theta_M\end{pmatrix}, \tag{2.31}$$

where

$$\sin 2\theta_M \equiv \frac{\sin 2\theta}{A_M} \tag{2.32}$$

$$\Delta m_M^2 \equiv \Delta m_{21}^2 A_M \tag{2.33}$$

$$A_M \equiv \sqrt{\left(\cos 2\theta \mp \frac{2EV_e}{\Delta m_{21}^2}\right)^2 + \sin^2 2\theta}, \tag{2.34}$$

and now the negative sign in A_M is for neutrinos and the positive sign for anti-neutrinos. As the electron number density goes to 0, so too does V_e and the vacuum solution is recovered.

From the form of this solution, it can be seen that the Hamiltonian takes the same form as that in vacuum oscillations, but with modified effective masses. Likewise, U_M has the same form as the 2 neutrino PMNS matrix, so θ_M can be considered the effective mixing angle. In the absence of neutrino oscillations (when $\theta = 0$), matter effects cannot "create" them. However, even for small angles θ, the matter effect can create a resonant effect pushing the effective mixing angle, θ_M, maximally to $45°$. This occurs when the term in parenthesis in the definition of A_M is 0 (eq. 2.34).

$$N_e^{res} = \frac{\Delta m_{21}^2 \cos 2\theta}{2\sqrt{2} G_F E} \tag{2.35}$$

In the case of 3 neutrinos, the same procedure is followed to diagonalize the Hamilton and obtain effective values for the various oscillation parameters. The effects are considerably more complicated, but the general effect is the same–matter changes the effective neutrino mass and alters the oscillation probability curves differently for neutrinos and anti-neutrinos. Under the same conditions that were used to calculate $P(\overset{(}{\bar{\nu}}\overset{)}{}_\mu \rightarrow \overset{(}{\bar{\nu}}\overset{)}{}_e)$ in sec. 2.3, the results can be simplified to a few basic replacements [36].

$$P(\overset{(}{\bar{\nu}}\overset{)}{}_\mu \rightarrow \overset{(}{\bar{\nu}}\overset{)}{}_e) = P_{atm}^M + 2\sqrt{P_{atm}^M}\sqrt{P_{sol}^M}\left(\cos\delta\cos\Delta_{32} \overset{(+)}{-} \sin\delta\sin\Delta_{32}\right) + P_{sol}^M \tag{2.36}$$

This is exactly the same form as eq. 2.25. The interesting effects are seen with how P_{atm}^M and P_{sol}^M differ from their respective vacuum counterparts.

$$\begin{aligned}
\sqrt{P_{atm}^M} &\equiv \sin\theta_{23}\sin 2\theta_{13}\frac{\sin(\Delta_{31} - aL)}{\Delta_{31} - aL}\Delta_{31} &(2.37)\\
\sqrt{P_{sol}} &\equiv \cos\theta_{23}\sin 2\theta_{12}\frac{\sin(aL)}{aL}\Delta_{21} &(2.38)
\end{aligned}$$

Here, $a \equiv \pm G_F N_e/\sqrt{2}$ where the positive sign is for neutrinos and the negative sign for anti-neutrinos. For the Earth, $|a| \approx 1/3500\,km$.

The combined effect that appears in eq.s 2.36, 2.37, and 2.38 due to the presence of matter plays an interesting role in the search for CP violation. The MSW effect by itself mimics CP violation as it alters oscillation probabilities for neutrinos and anti-neutrinos differently. Depending on the value of δ that nature has chosen, the differences in oscillation probabilities due to the CP violation angle and the MSW effect can either compound or cancel out.

2.5 Current Measurements

Most of the free parameters in the PMNS matrix have been measured by various solar, atmospheric, accelerator, and reactor neutrino experiments. However, any given neutrino experiment does not have sensitivity to all of the oscillation parameters. Instead, experiments are sensitive to specific angles based on their baseline and the energies of the neutrinos they observe. Solar neutrino experiments, such as GALLEX, SAGE, Super-K, and SNO, measure neutrinos with energies on the order of several MeV after a very long baseline, and are most sensitive to θ_{12} and Δm^2_{21}. Due to the strong MSW effect within the Sun, solar neutrino experiments also determined the ordering of mass states ν_1 and ν_2; ν_2 is defined as the heavier state. Atmospheric neutrino experiments, such as Super-K, SNO, and MINOS, measure neutrinos generated by cosmic ray collisions with the Earth's atmosphere, and are sensitive to θ_{23} and Δm^2_{32}.

Reactor neutrino experiments, such as Chooz, Double Chooz, RENO, and Daya Bay, measure $\bar{\nu}_e$ generated by nearby nuclear reactors. Like solar neutrinos, reactor neutrinos have energies on the order of a few MeV. By measuring these neutrinos with a short baseline ($O(1km)$), the 2 neutrino approximation is valid, so the oscillation probability can be approximated as:

$$P(\bar{\nu}_e \to \bar{\nu}_e) \approx 1 - \sin^2 2\theta_{13} \sin^2 \Delta_{31}. \tag{2.39}$$

Daya Bay made the first nonzero measurement of θ_{13} in 2012, reporting a value of $\sin^2 2\theta_{13} = 0.092 \pm 0.016$ (stat) $\pm\ 0.005$ (syst) after taking just 55 days of data [37]. This result excluded a zero value for θ_{13} at 5.2σ and is shown in Fig. 2.4. Since that result, the limits have only continued to improve, and the leading measurement still comes from Daya Bay.

Accelerator neutrino experiments, such as MINOS, T2K, and NOνA, begin with a beam of nearly pure $\overset{(-)}{\nu}_\mu$ and search for both a disappearance of $\overset{(-)}{\nu}_\mu$ and appearance of other neutrino flavors. These experiments are sensitive to θ_{13}, θ_{23}, Δm^2_{32}, and δ. The experiments that have the largest matter effect are the most sensitive to δ and the mass hierarchy.

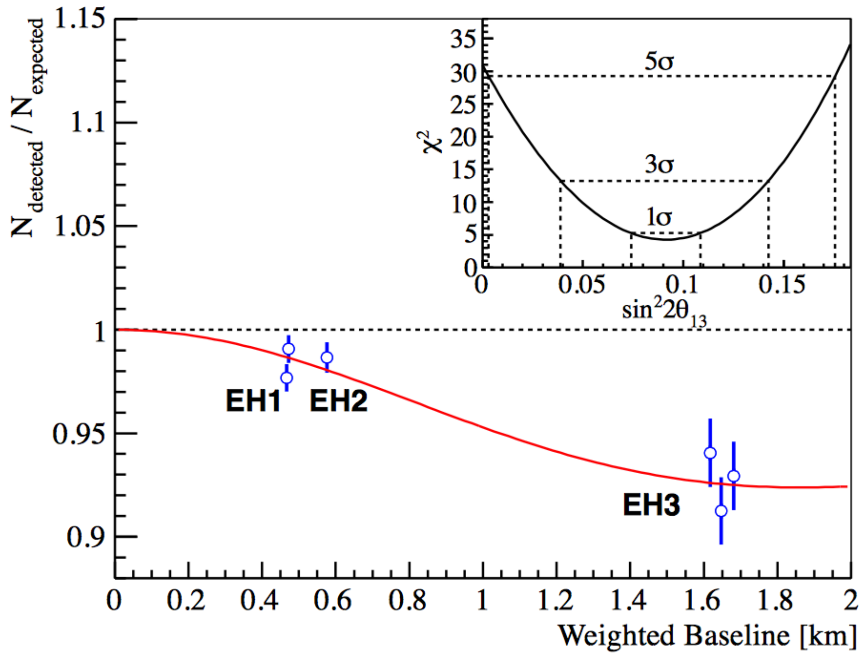

Figure 2.4: First measurement of θ_{13} from Daya Bay [37]. The points show the ratio of observed to expected events assuming $\theta_{13} = 0$. Each point is a measurement at a different detector. The inset in the upper corner shows the χ^2 value vs value of $\sin^2 2\theta_{13}$, and excludes $\theta_{13} = 0$ at greater than 5σ.

Global fits to the combined data of these (and other) neutrino experiments have been performed and summarized in [31, 38]; the best fit values are shown in Table 2.1. While most of the parameters have been measured with good precision, there are still a few lingering questions. From the table it is clear that a much better measurement on the CP violation angle is needed. The mass hierarchy still needs to be definitively measured as well. The other main question is whether θ_{23} is maximal, and if not, whether it is in the lower or upper octant.

Current and next generation reactor experiments have a great outlook to answer these outstanding questions. Making use of the MSW effect, the ν_e and $\bar{\nu}_e$ appearance results from experiments like T2K and NOνA could simultaneously measure δ, the mass hierarchy, and θ_{23} octant. The prospects for NOνAto make these measurements are shown in Fig. 2.5. The first analysis results from NOνA [39, 40] were published after taking about 10% of the experiments design statistics and already show promise. The NOνA measurement for δ, shown in Fig. 2.6, provide a hint toward the normal hierarchy and eliminate portions of δ space at 90% confidence.

Table 2.1: Current status of best fit oscillation parameters, from [31, 38]. The last column shows the allowed values within a 3σ range, with the exception of δ, which is shown at a 2σ range. This is because the current global best fit for δ still allows the full range from 0 to 2π at 3σ. NOνA should vastly improve the limits on δ.

Parameter		Best-Fit $(\pm 1\sigma)$	3σ Range
Δm^2_{21} $[10^{-5}$ eV²$]$		$7.54^{+0.26}_{-0.22}$	$6.99 - 8.18$
$\lvert\Delta m^2\rvert$ $[10^{-3}$ eV²$]$	NH	2.43 ± 0.06	$2.23 - 2.61$
	IH	2.38 ± 0.06	$2.19 - 2.56$
$\sin^2\theta_{12}$		0.308 ± 0.017	$0.259 - 0.359$
$\sin^2\theta_{23}$	NH	$0.437^{+0.033}_{-0.023}$	$0.374 - 0.628$
	IH	$0.455^{+0.039}_{0.031}$	$0.380 - 0.641$
$\sin^2\theta_{13}$	NH	$0.0234^{+0.0020}_{-0.0019}$	$0.0176 - 0.0295$
	IH	$0.0240^{+0.0019}_{-0.0022}$	$0.0178 - 0.0298$
δ/π $(2\sigma$ range)	NH	$1.39^{+0.38}_{-0.27}$	$(0.00 - 0.16) \oplus (0.86 - 2.00)$
	IH	$1.31^{+0.29}_{-0.33}$	$(0.00 - 0.02) \oplus (0.70 - 2.00)$

2.6 Sterile Neutrinos

2.7 Neutrino Mass in the Standard Model

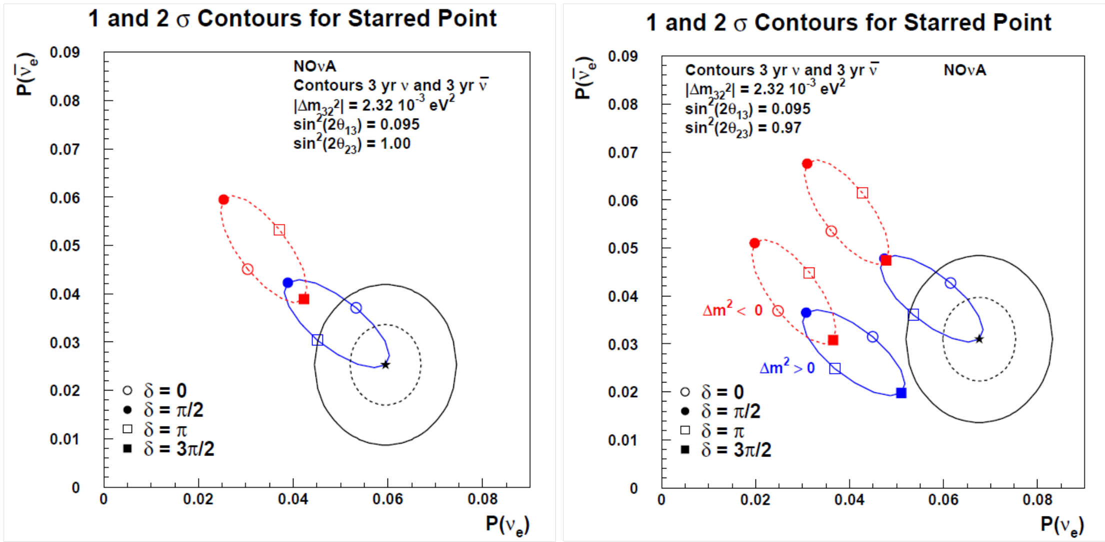

Figure 2.5: Probability of ν_e appearance versus $\bar{\nu}_e$ appearance at NOνA. The blue ellipses are for the normal hierarchy; the red ellipses are for the inverted hierarchy. The starred points show a possible measurement NOνA could make. The matter effect can either constructively or destructively combine with the CP violation effect. A larger matter effect, further separates the two mass hierarchy ellipses. This corresponds to neutrinos passing through more matter. On the left, θ_{23} is assumed to be 45° for maximal mixing, purely showcasing the interference between the matter and CP violation effects. On the right, θ_{23} is non-maximal, showing how the dependence on θ_{23} affects both ellipses in the same way.

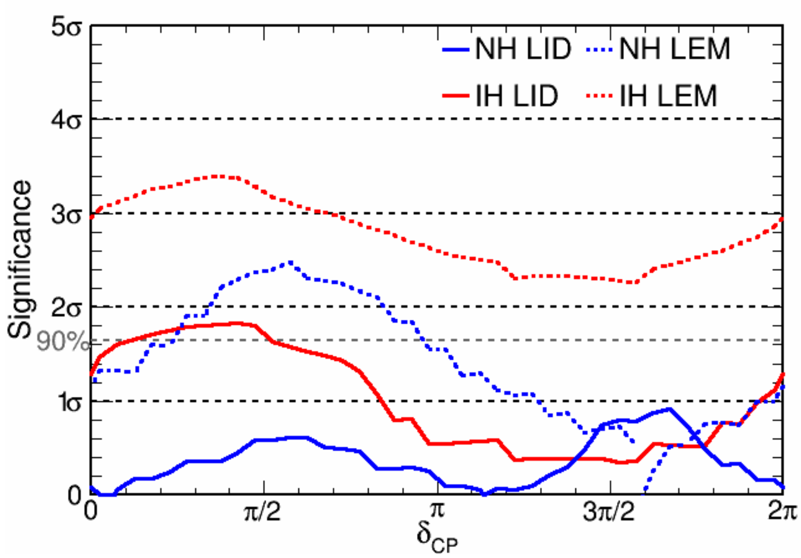

Figure 2.6: First measurement of δ from NOνA [39]. The plot shows the significance of the difference between the observed and predicted number of events as a function of delta. NOνA used a primary and secondary selection technique, the primary (secondary) technique is shown as the solid (dotted) line. The secondary selection disfavors the inverted hierarchy for all values of δ.

3

The NOνA Experiment

4

Experiment Simulation

4.1 Introduction

4.2 Flux Simulation

4.3 Detector Simulation

5

Event Reconstruction

5.1 Reconstruction Chain

5.2 Calibration

6

Neutral Current Event Selection

6.1 Preselection

6.2 CVN Based Selection

6.3 Standard PID Cross Check

6.4 Cosmic Rejection

7

Neutral Current Spectrum Prediction

Any rigorous scientific analysis must have a well defined analysis procedure. This chapter describes the bulk of that procedure for the FD NC disappearance analysis. The methods presented use the NC event selection discussed in ch. 6 to predict the FD energy spectrum.

7.1 The CAFAna Analysis Chain

The analysis presented in this thesis was performed in a software framework called CAFAna that analyzes Common Analysis Format files, or CAFs. The design principles of CAFAna recognize that all neutrino analyses have to perform essentially the same tasks, such as decomposing a detector spectrum into different components or applying oscillation weights to a particular event spectrum. A given task might have multiple implementations, but while the inner details are different, the number and type of end products are the same. Thus CAFAna has a fixed general analysis chain with the ability to easily swap specific implementations of any given piece of the chain.

The general analysis chain shown in Fig. ?? illustrates how a near to far detector analysis can be neatly separated into smaller components that

7.2 Near Detector Decomposition

7.3 Extrapolation

7.4 Far Detector Prediction

8

Analysis Results and Systematic Errors

8.1 Fitting Method

8.2 Systematic Errors

As with any experiment, NOνA is sensitive to a number of systematic effects. To combat this, NOνA was designed with two functionally identical detectors, so that Near Detector data can be used to constrain or correct the Far Detector prediction. Since many effects such as beam and cross section uncertainties affect the spectra at both detectors in a similar or the same way, this two detector technique leads to the reduction of these systematic errors. Other effects, such as Near Detector rock event contamination, require a data driven technique to quantify.

The general technique for analyzing systematic errors was to run the full extrapolation chain and generate a predicted spectrum with and without a systematic effect applied. Each given systematic effect was used to shift the MC simulation at one or both detectors as appropriate. The resulting difference between the shifted and nominal spectra was quantified as a systematic error.

The systematic effects analyzed included uncertainties arising from the beam, GENIE simulation, Birks-Chou light yield simulation, calibration, detector geometry simulation, light level effects, bias from the ND containment, ND rock event contamination, ND data/MC spectrum and hadronic energy differences, MC statistics, and overall normalization. The rest of this section discusses each of these effects in greater detail.

8.2.1 Beam

The NOνA MC simulation involves a fully detailed model of the NuMI beam process in an attempt to create the most realistic MC possible, but systematic errors can result from any mismatch between simulation and reality. The NOνA Beam Working Group performed studies to assess the effect that uncertainties in the simulation can have on the neutrino flux [41]. These studies included the effects of incorrectly modeling various parts of the beam transport and the effects of uncertainties in hadron production arising from fixed target experiments.

To quantify the systematic error caused by these beam uncertainties, a sample flux was generated using a systematic shift and compared to the nominal flux via a simple ratio. Results were generated separately for each neutrino flavor and for each detector. The ratios were used to modify the MC from the full simulation used as inputs to the extrapolated prediction. Finally, the shifted FD prediction was compared to the nominal prediction, with any differences being taken as the systematic error. At the end of this process, the individual errors were added in quadrature. Errors were calculated for the following systematics:

- Beam position on target varied by $\pm 0.5\,mm$ in X
- Beam position on target varied by $\pm 0.5\,mm$ in Y
- Beam spot size varied by $\pm 0.2\,mm$ in both X and Y
- Target position varied by $+2\,mm$ in Z
- Horn current varied $\pm 1\,kA$

- Horn 1 position varied by $\pm 2\,mm$ in both X and Y
- Horn 2 position varied by $\pm 2\,mm$ in both X and Y
- Horn magnetic field changed from linear to exponential distribution
- Comparison between FLUKA and G4NuMI
- Comparison between FLUKA and NA49

Hadron production uncertainties were combined in quadrature before being provided as weights, so this is evaluated as single systematic error. The percentage difference due to each systematic is shown in Table 8.1, and the full error envelopes for NC signal and background are shown in Fig. 8.1. The beam systematics had an overall effect of $TODO\%$ on the NC signal and $TODO\%$ on the background.

Table 8.1: The percentage difference between the shifted and nominal predictions for the number of FD events due to beam systematics.

Systematic	NC Difference (%)	Background Difference (%)
Beam Position, X		
Beam Position, Y		
Beam Spot Size		
Target Position		
Horn Current		
Horn 1 Position		
Horn 2 Position		
Horn B Field		
Hadron Productions		
Combined		

8.2.2 Birks-Chou Light Yield Simulation

The NOνA MC simulation employs the Birks-Chou Law to model the relationship between scintillator light yield, LY, and particle energy deposition rate, $\frac{dE}{dx}$ [42].

$$LY = A \frac{\frac{dE}{dx}}{1 + k_B \frac{dE}{dx} + k_C \left(\frac{dE}{dx}\right)^2} \tag{8.1}$$

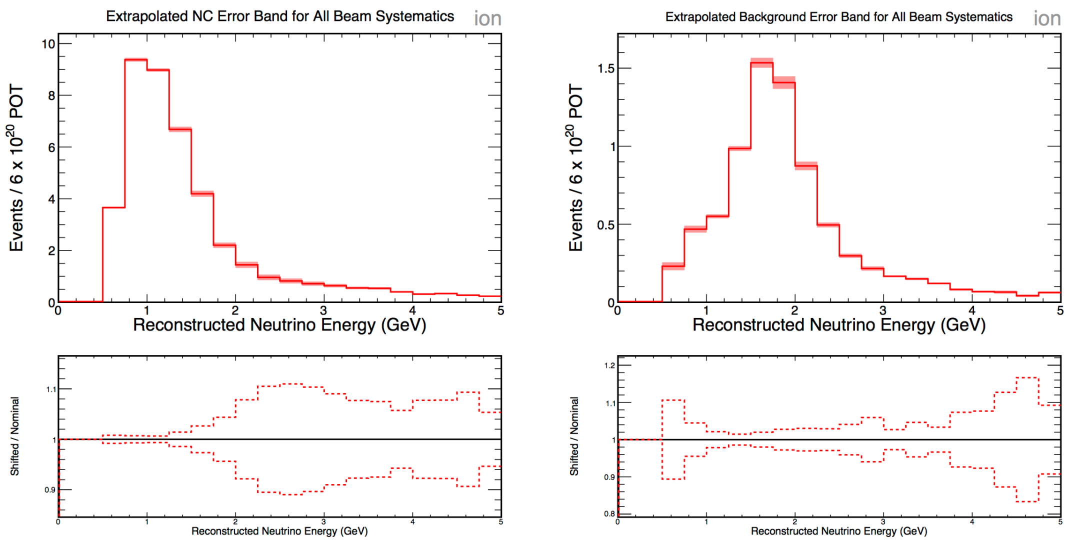

Figure 8.1: Systematic error envelope on the NC signal (left) and background (right) event spectra, after extrapolation. The envelope was calculated by adding in quadrature the larger of $|+1\sigma|$ and $|-1\sigma|$ for each individual systematic.

This formula encapsulates the known light yield quenching that occurs for particles with a high energy deposition rate. The constants k_B and k_C are dependent on the scintillator material and had to be estimated for NOνA as no measurement existed for the particular material used in this experiment. A study was performed comparing the energy deposition at the end of proton tracks in the ND for both data and MC to find parameters that would generate agreement between the two [43]. The results of the study were $k_B = 0.04\,\text{cm/MeV}$ and $k_C = -0.0005\,(\text{cm/MeV})^2$.

The systematic error based on the Birks-Chou light yield simulation was quantified by comparing the nominal FD prediction to predicted spectra using alternative Birks-Chou parameter constants. The values reported in the study from [43] were much larger than other typical measurements, so two MC samples were generated with more traditional values, one with $k_B = 0.01\,\text{cm/MeV}$ called BirksB, the other with $k_B = 0.02\,\text{cm/MeV}$ called BirksC, both with $k_C = 0$. Shifted FD event spectra were predicted by extrapolating the same set of ND data as the nominal prediction, but using the MC with alternative Birks-Chou model parameters. The error was taken as the percentage difference between the nominal and shifted predictions. Table 8.2 shows the percentage differences from both MC samples; fig. 8.2 shows the shifted event spectra compared to nominal. Instead of combining the individual errors in quadrature, the shifted sample with the larger overall difference from the TODO model taken as the systematic error, which had a $TODO\%$ effect on the NC signal, and a $TODO\%$ effect on the background.

Table 8.2: The percentage difference between the shifted and nominal predictions for the number of FD events due to extrapolation using MC with alternative Birks-Chou model parameters.

Model	NC Difference (%)	Background Difference (%)
BirksB		
BirksC		

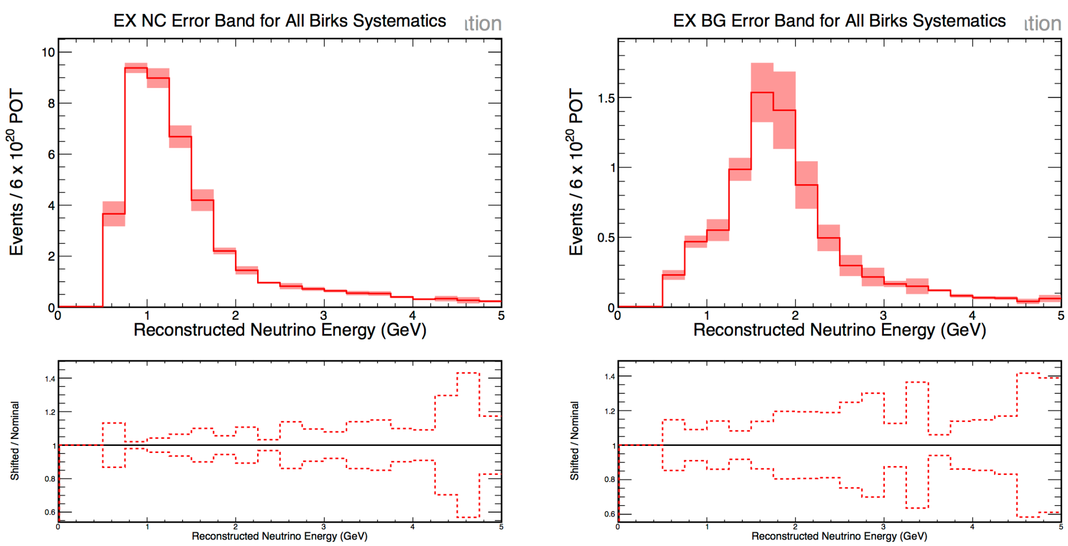

Figure 8.2: Shifted FD predictions due to extrapolation of ND data with MC using different Birks-Chou parameter values. The NC signal spectrum is on the left; the background spectrum is on the right.

8.2.3 Calibration

The calibration procedure is designed to make a constant energy response both across each detector and between the two, but any problem can introduce a systematic error. This error was evaluated by studying various MC samples with an engineered miscalibration. The effects studied included a miscalibration that varied as a function of the cell length and an overall scale miscalibration. The functional miscalibration was studied separately between the X and Y views of the detector. The scale miscalibration was applied as a 5% effect both up and down at each detector.

The systematic error was evaluated in two regimes. The first applied the same miscalibration to the MC at both detectors, and a shifted prediction was then generated using these shifted as inputs into the extrapolation. This procedure was followed for each type of miscalibration, and all of these systematics were added in quadrature at the end. The overall scale miscalibration was also applied as a miscalibration to a single detector to measure the effect of a missed absolute calibration. A shifted prediction was then generated as above, but with this procedure only the maximum overall effect was used as the systematic error that was then added in quadrature with the systematics from above. Table 8.3 shows the percentage difference for each of the calibration systematics. The overall error was $TODO\%$ on the NC signal and $TODO\%$ on the background.

Table 8.3: The percentage difference between the shifted and nominal predictions for the number of FD events due to deliberately applied miscalibrations. For the flat scale miscalibration applied to 1 detector, the largest overall effect from the scale TODO at the ND was taken as the systematic.

Miscalibration	NC Difference (%)	Background Difference (%)
Miscalibration applied to both detectors:		
Sloped X		
Sloped Y		
Flat Scale Up		
Flat Scale Down		
Miscalibration applied to one detector:		
Flat Scale Up, ND		
Flat Scale Down, ND		
Flat Scale Up, FD		
Flat Scale Down, FD		

8.2.4 Detector Alignment

The NOνA simulation involves a detailed model of the detectors that uses survey data to place individual planes. Of course, there is always some uncertainty in any measurement. In the past, NOνA MC was generated using an 'ideal' geometry that had planes lined up in a perfect fashion. To quantify the systematic error due to detector alignment uncertainty, a small sample of FD MC was generated with these ideal conditions, and a shifted prediction was created using this MC. The percentage difference was taken as the systematic error, for a $TODO\%$ effect on the NC signal and a $TODO\%$ effect on the background.

8.2.5 GENIE Simulation

Neutrino interactions in the NOνA simulation are generated using GENIE [44], a generator that involves a detailed physics modeling of cross sections, hadronization, and final state interactions. GENIE includes a plethora of parameters that alter individual physics input quantities, with the parameters themselves acting as systematic uncertainties, either dialing up or down a particular quantity by a standard deviation recommended by the GENIE authors.

The systematic uncertainties from physics modeling were evaluated by using the GENIE parameters as event reweights. Nominal MC was produced using the parameters and weights as provided by the GENIE authors, but also included a table of weights to modify an events 'worth' based on how much the different GENIE parameters shifted. Using the reweight table, a nominal FD prediction was produced from the default MC, and a shifted prediction was produced for each of the parameters provided by GENIE. The percentage difference was taken as the systematic error for the particular parameter. Table 8.4 lists all of the parameters considered for the systematic study, and the associated error. Fig. 8.3 shows the final systematic error envelope. The combined systematic error, adding the individual contributions in quadrature, was $TODO\%$ for the NC signal and $TODO\%$ for the background.

Table 8.4: The systematic error, in percentage difference, for each GENIE systematic parameter. The description and standard deviations come from ref. [44].

Parameter Description and Standard Deviation		NC Diff. (%)	Bkg. Diff. (%)
Axial mass for NC elastic	$\pm 25\%$		
Strange axial form factor η for NC elastic	$\pm 30\%$		
Normalization Factor for CCQE			
Normalization Factor for CCQE			
CCQE Pauli suppression (via changes in Fermi level k_F)	$\pm 35\%$		
Choice of CCQE vector form factors (BBA05 $\leftrightarrow$ Dipole)	-		
CCQEMomDistroFGtoSF			
Axial mass for CC resonance neutrino production	$\pm 20\%$		
Vector mass for CC resonance neutrino production	$\pm 10\%$		
Axial mass for NC resonance neutrino production	$\pm 20\%$		
Vector mass for NC resonance neutrino production	$\pm 10\%$		
Axial mass for CC and NC coherent pion production	$\pm 50\%$		
Nuclear size param controlling π absorption in RS model	$\pm 10\%$		
Non-resonance bkg in νp CC1π reactions	$\pm 50\%$		
Non-resonance bkg in νp CC2π reactions	$\pm 50\%$		

Parameter Description and Standard Deviation		NC Diff. (%)	Bkg. Diff. (%)
Non-resonance bkg in νn CC1π reactions	$\pm 50\%$		
Non-resonance bkg in νn CC2π reactions	$\pm 50\%$		
Non-resonance bkg in νp NC1π reactions	$\pm 50\%$		
Non-resonance bkg in νp NC2π reactions	$\pm 50\%$		
Non-resonance bkg in νn NC1π reactions	$\pm 50\%$		
Non-resonance bkg in νn NC2π reactions	$\pm 50\%$		
Non-resonance bkg in $\bar{\nu} p$ CC1π reactions	$\pm 50\%$		
Non-resonance bkg in $\bar{\nu} p$ CC2π reactions	$\pm 50\%$		
Non-resonance bkg in $\bar{\nu} n$ CC1π reactions	$\pm 50\%$		
Non-resonance bkg in $\bar{\nu} n$ CC2π reactions	$\pm 50\%$		
Non-resonance bkg in $\bar{\nu} p$ NC1π reactions	$\pm 50\%$		
Non-resonance bkg in $\bar{\nu} p$ NC2π reactions	$\pm 50\%$		
Non-resonance bkg in $\bar{\nu} n$ NC1π reactions	$\pm 50\%$		
Non-resonance bkg in $\bar{\nu} n$ NC2π reactions	$\pm 50\%$		
A_{HT} higher-twist param in BY model scaling variable ξ_w	$\pm 25\%$		
B_{HT} higher-twist param in BY model scaling variable ξ_w	$\pm 25\%$		
C_{V1u} u valence GRV98 PDF correction param in BY model	$\pm 30\%$		
C_{V2u} u valence GRV98 PDF correction param in BY model	$\pm 40\%$		
Inclusive CC cross-section normalization factor			
$\bar{\nu}/\nu$ CC ratio			
DIS nuclear			
Pion transverse momentum (p_T) for $N\pi$ states in AGKY	-		
Pion Feynman x (x_F) for $N\pi$ states in AGKY	-		
Hadron formation zone	$\pm 50\%$		
Pion angular distribution in $\Delta \to \pi N$ (isotropic $\leftrightarrow$ RS)	-		
Branching ratio for radiative resonance decays	$\pm 50\%$		
Branching ratio for single-η resonance decays	$\pm 50\%$		
Nucelon mean free path (total rescattering probability)	$\pm 20\%$		
Nucleon charge exchange probability	$\pm 50\%$		
Nucleon elastic reaction probability	$\pm 30\%$		
Nucleon inelastic reaction probability	$\pm 40\%$		
Nucleon absorption probability	$\pm 20\%$		
Nucleon π-production probability	$\pm 20\%$		
π mean free path (total rescattering probability)	$\pm 20\%$		
π charge exchange probability	$\pm 50\%$		
π elastic reaction probability	$\pm 10\%$		
π inelastic reaction probability	$\pm 40\%$		
π absorption probability	$\pm 20\%$		
π π-production probability	$\pm 20\%$		
MEC event scale	$+50\%$		
RPA event weight	Varied		

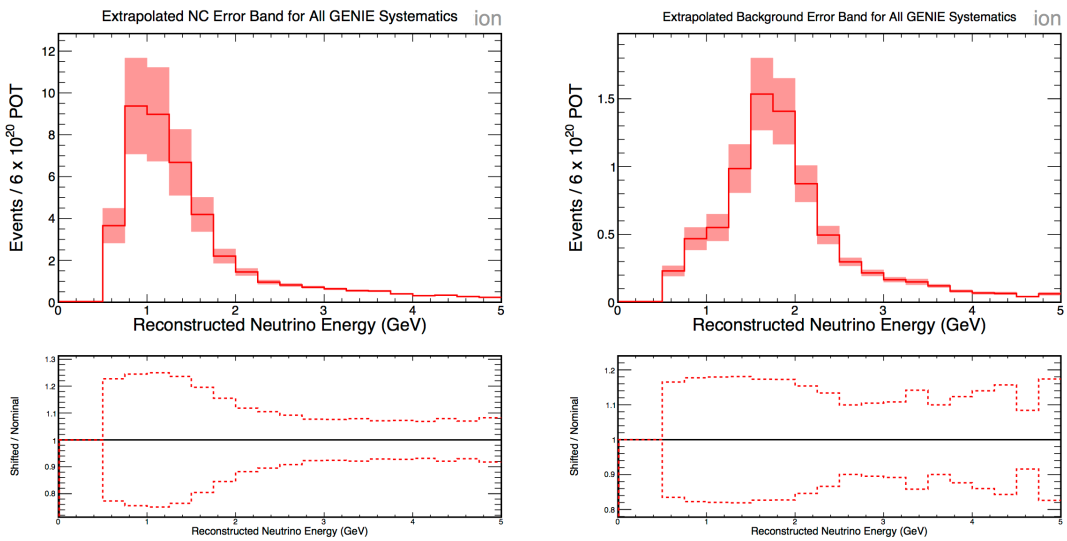

Figure 8.3: Systematic error envelope on the NC signal (left) and background (right) event spectra, after extrapolation. The envelope was calculated by adding in quadrature the larger of $|+1\sigma|$ and $|-1\sigma|$ for each individual systematic.

8.2.6 Light Level Effects

8.2.7 ND Containment

The ND does not see an effective point source of neutrinos like the FD due to its proximity to the beam source. As a result, the neutrino flux is not uniform across the detector, and so the energy spectrum of neutrinos seen by the two NOνA detectors is slightly different. To study the effect this has on the extrapolated prediction, multiple predicted FD spectra were generated using subsamples of the ND. The fiducial volume of the ND was split in half along each axis, and split into an inner and outer half (the overall containment criteria was left in tact). The extrapolation was performed using each of these 'half detectors.' The error was taken as the percentage difference from the shifted prediction to the nominal. Table 8.5 shows the results from each of these extrapolations and fig. 8.4 show the shifted spectra. Like the Birks-Chou systematic, the largest overall difference was taken as the systematic error for a $TODO\%$ effect on the NC signal and a $TODO\%$ effect on the background.

Table 8.5: The percentage difference between the shifted and nominal predictions for the number of FD events after extrapolation using half of the fiducial volume at the ND.

ND Half	NC Difference (%)	Background Difference (%)
West (+X)		
East (-X)		
Top (+Y)		
Bottom (-Y)		
Front (Low Z)		
Back (High Z)		
Inner (Low |X|, |Y|)		
Outer (High |X|, |Y|)		

8.2.8 ND Rock Event Contamination

The MC simulation does include neutrino interactions that occur in the rock that surrounds the ND. These events often leak into the detector volume, and while most of them are cut away by fiducial and containment cuts, there are some that remain. Those events that do remain cannot be reconstructed properly as their origins are outside of the detector.

The systematic error that is incurred due to the rock event contamination was estimated by predicting the FD event spectrum from an extrapolation with rock events removed by MC truth and comparing to the nominal predicted spectrum. The events were only removed from the ND MC sample, requiring that the true neutrino vertex was inside the detector to remain. The shifted spectra are shown in Fig. 8.5. This systematic amounted to an overall $TODO\%$ shift on the NC signal spectrum and a $TODO\%$ shift on the background spectrum.

8.2.9 ND Data/MC

8.2.10 Noise Model

8.2.11 MC Statistics

In a perfect world, there would be enough MC statistics that this section would be unnecessary, but alas, a perfect world this is not. To estimate the systematic error due to MC statistics, the MC was split

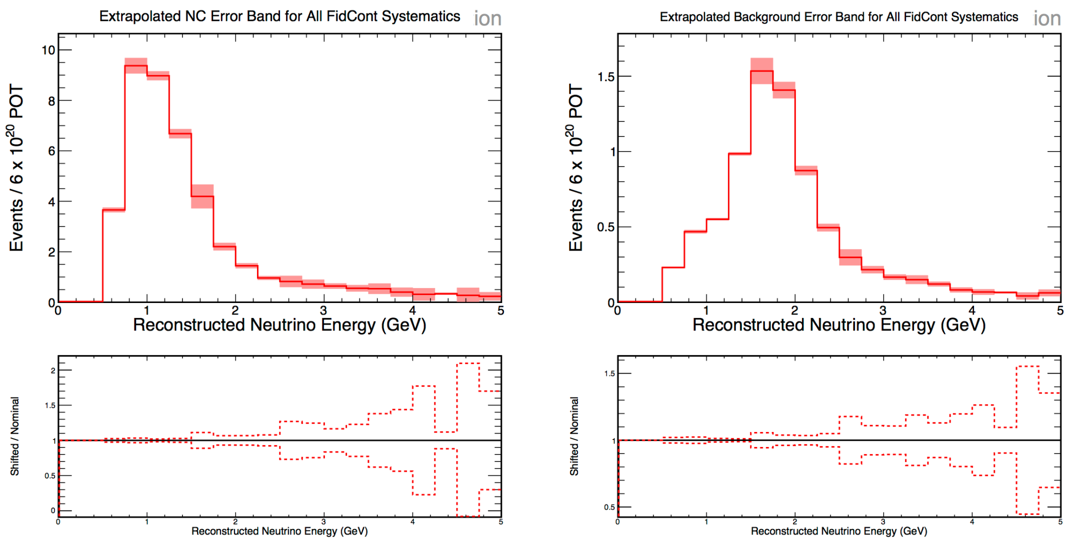

Figure 8.4: Shifted FD predictions after extrapolation using only half of the ND fiducial volume. The NC signal spectrum is on the left; the background spectrum is on the right.

into five uniformly sized samples, and each was used to extrapolate the same set of ND data. One of the resultant predicted FD spectra was labeled as nominal, and the other four were compared to this. The bin by bin differences were taken as the error between the nominal spectrum and the 'shifted' spectrum. To come up with an overall uncertainty, all of the errors were added in quadrature and the result was divided by the square root of the number of samples, or $\sqrt{4} = 2$. The result was a $TODO\%$ error on the NC signal spectrum and a $TODO\%$ error on the background spectrum.

8.2.12 Overall Normalization

Several independent effects contributed to an overall normalization systematic error. A 0.5% error on the POT counting came from a small difference in the two toroids that determine the POT in a spill [41]. Uncertainties in the masses of the various parts of the NOνA detectors contributed another error of 0.7% [45]. Finally, a study of the reconstruction efficiency between ND data and MC showed a $TODO\%$ difference [46], which was taken directly as a contribution to the normalization error. These three effects were combined in quadrature and constituted a $TODO\%$ systematic error.

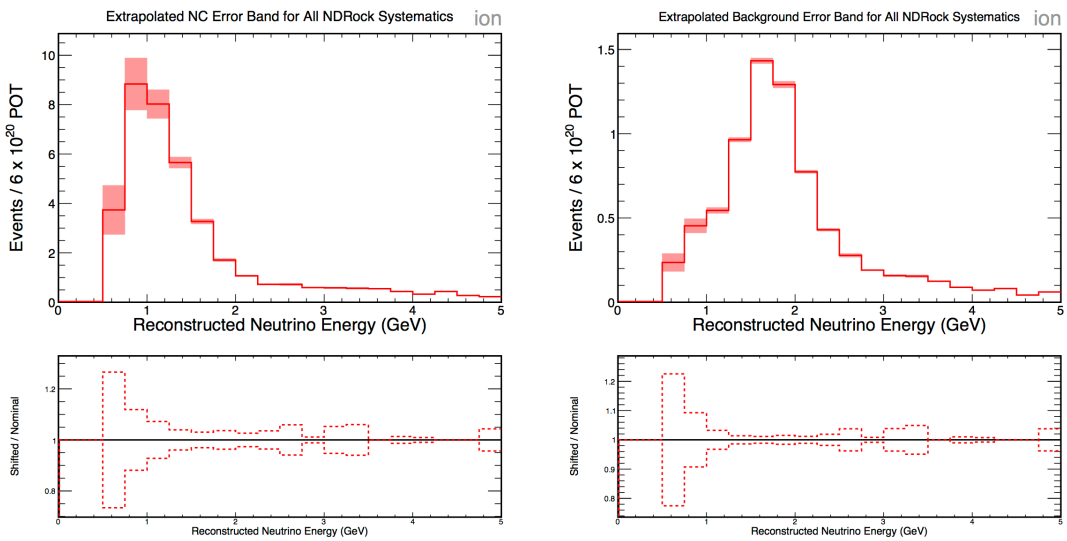

Figure 8.5: Shifted vs nominal spectra for the NC signal (left) and background (right). The shifted spectra are extrapolated after removal of rock events in the ND MC by truth.

8.2.13 Systematic Error Summary

Table 8.6 shows a summary of all of the systematics, as well as an overall error. The overall error was calculated by summing the error from each row in quadrature. The final systematic error on the NC signal is $TODO\%$ and the error on the background is $TODO\%$.

8.3 Results

Table 8.6: A summary of the individual systematic errors for the NC disappearance analysis. The errors are percentage differences between the nominal and shifted predicted spectra.

Systematic	NC Difference (%)	Background Difference (%)
Beam		
Birks-Chou		
Calibration		
Detector Alignment		
GENIE		
Light Levels		
ND Containment		
ND Rock Contamination		
ND Data/MC		
MC Statistics		
Combined		

9

Conclusions and Future Improvements

9.1 Conclusions

The results of this analysis are consistent with no sterile neutrinos.

9.2 Future Improvements

References

[1] W. Pauli. Letter to a physicists' gathering at tubingen, 1930.

[2] J. Chadwick. Possible existence of a neutron. *Nature*, 192:312, 1932.

[3] E. Fermi. Versuch einer theorie der β-strahlen. *Zeitschrift für Physik*, 88:161–177, 1934.

[4] F. Reines and C. L. Cowan. Detection of the free neutrino. *Physical Review*, 92:830–831, 1953.

[5] C. L. Cowan, F. Reines, F. B. Harrison, H. W. Kruse, and A. D. McGuire. Detection of the free neutrino: A confirmation. *Science*, 124:103–104, 1956.

[6] G. Danby et al. Observation of high-energy neutrino reactions and the existence of two kinds of neutrinos. *Physical Review Letters*, 9:36–44, 1962.

[7] DONUT Collaboration, K. Kodama et al. Observation of tau neutrino interactions. *Physics Letters B*, 504:218–224, 2001.

[8] B. Pontecorvo. Mesonium and anti-mesonium. *Soviet Journal of Experimental and Theoretical Physics*, 6:429, 1957.

[9] R. Davis, Jr., D. S. Harmer, and K. C. Hoffman. Search for neutrinos from the sun. *Physical Review Letters*, 20:1205–1209, 1968.

[10] J. N. Bahcall, N. A. Bahcall, and G. Shaviv. Present status of the theoretical predictions for the ^{37}Cl solar-neutrino experiment. *Physical Review Letters*, 20:1209–1212, 1968.

[11] V. Gribov and B. Pontecorvo. Neutrino astronomy and lepton charge. *Physics Letters B*, 28:493–496, 1969.

[12] K.S. Hirata et al. Observation of B-8 solar neutrinos in the Kamiokande-II detector. *Physical Review Letters*, 63:16–19, 1989.

[13] A. I. Abazov et al. Search for neutrinos from the sun using the reaction ^{71}Ga (ν_e, e^-) ^{71}Ge. *Physical Review Letters*, 67:3332–3335, 1991.

[14] P. Anselmann et al. Solar neutrinos observed by GALLEX at Gran Sasso. *Physics Letters B*, 285:376–389, 1992.

[15] K.S. Hirata et al. Observation of a small atmospheric ν_μ/ν_e ratio in Kamiokande. *Physical Letters B*, 280:146–152, 1992.

[16] Y. Fukuda et al. Evidence for oscillation of atmospheric neutrinos. *Physical Review Letters*, 81:1562–1567, 1998.

[17] Q. R. Ahmad et al. Direct evidence for neutrino flavor transformation from neutral-current interactions in the sudbury neutrino observatory. *Physical Review Letters*, 89:011301, 2002.

[18] ALEPH Collaboration, DELPHI Collaboration, L3 Collaboration, OPAL Collaboration, SID Collaboration, LEP Electroweak Working Group, SID Electroweak Group, Heavy Flavour Group. Precision electroweak measurements on the Z resonance. *Physics Reports*, 427:218–224, 2006.

[19] C. Athanassopoulos et al. Candidate events in a search for anti-muon-neutrino –> anti-electron-neutrino oscillations. *Physical Review Letters*, 75:2650–2653, 1995.

[20] A. A. Aguilar-Arevalo et al. A search for electron neutrino appearance at the $\Delta m^2 \sim 1$ eV^2 scale. *Physical Review Letters*, 98:231801, 2007.

[21] A. A. Aguilar-Arevalo et al. Improved search for $\bar{\nu}_\mu \rightarrow \bar{\nu}_e$ oscillations in the MiniBooNE experiment. *Physical Review Letters*, 110:161801, 2013.

[22] B. Armbruster et al. Upper limits for neutrino oscillations $\bar{\nu}_\mu \rightarrow \bar{\nu}_e$ from muon decay at rest. *Physical Review D*, 65:112001, 2002.

[23] P. Astier et al. Search for $\nu_\mu \rightarrow \nu_e$ oscillations in the NOMAD experiment. *Physics Letters B*, 570:19–31, 2003.

[24] K. Abe et al. Limits on sterile neutrino mixing using atmospheric neutrinos in Super-Kamiokande. *Physical Review D*, 91:052019, 2015.

[25] F. P. An et al. Search for a light sterile neutrino at Daya Bay. *Physical Review Letters*, 113:141802, 2014.

[26] K. Abe et al. Search for short baseline ν_e disappearance with the T2K near detector. *Physical Review D*, 91:051102, 2015.

[27] P. Adamson et al. Active to sterile neutrino mixing limits from neutral-current interactions in minos. *Physical Review Letters*, 107:011802, 2011.

[28] Z. Maki, M. Nakagawa, and S. Sakata. Remarks on the unified model of elementary particles. *Progress of Theoretical Physics*, 28:870–880, 1962.

[29] J. Rich. Quantum mechanics of neutrino oscillations. *Physical Review D*, 48:4318–4325, 1993.

[30] B. Kayser. On the quantum mechanics of neutrino oscillation. *Physical Review D*, 24:110–116, 1981.

[31] K. A. Olive et al. Review of particle physics. *Chinese Physics C*, 38:090001, 2014.

[32] O. Mena and S. Parke. Unified graphical summary of neutrino mixing parameters. *Physical Review D*, 69:117301, 2004.

[33] E. Niner. *Observation of Electron Neutrino Appearance in the NuMI Beam with the NOνA Experiment*. PhD thesis, Indiana University, 2015.

[34] L. Wolfenstein. Neutrino oscillations in matter. *Physical Review D*, 17:2369–2374, 1978.

[35] S. P. Mikheev and A. Y. Smirnov. Resonance enhancement of oscillations in matter and solar neutrino spectroscopy. *Soviet Journal of Nuclear Physics*, 42:913–917, 1985.

[36] H. Nunokawa, S. Parke, and J. W. F. Valle. CP violation and neutrino oscillations. *Progress in Particle and Nuclear Physics*, 60:338–402, 2008.

[37] F. P. An et al. Observation of electron-antineutrino disappearance at Daya Bay. *Physical Review Letters*, 108:171803, 2012.

[38] F. Capozzi et al. Status of three-neutrino oscillation parameters, circa 2013. *Physical Review D*, 89:093018, 2014.

[39] P. Adamson et al. First measurement of electron-neutrino appearance in NOvA. *Physical Review Letters*, 2016.

[40] P. Adamson et al. First measurement of muon-neutrino disappearance in NOvA. *Physical Review D Rapid Communications*, 93:051104, 2016.

[41] H. Duyang et al. A technote describing the derivation and size of numi flux uncertainties used in the first analyses. NOνA Internal Document 13584.

[42] C. N. Chou. The nature of the saturation effect of fluorescent scintillators. *Physical Review*.

[43] D. Pershey. Birks-chou parameter selection. NOνA Internal Document 13158.

[44] C. Andreopoulos et al. The GENIE neutrino monte carlo generator: Physics and user manual. `http://arxiv.org/abs/1510.05494`.

[45] N. Raddatz. Fiducial mass systematic. NOνA Internal Document 13237.

[46] A. Markowitz. Todo. NOνA Internal Document TODO.

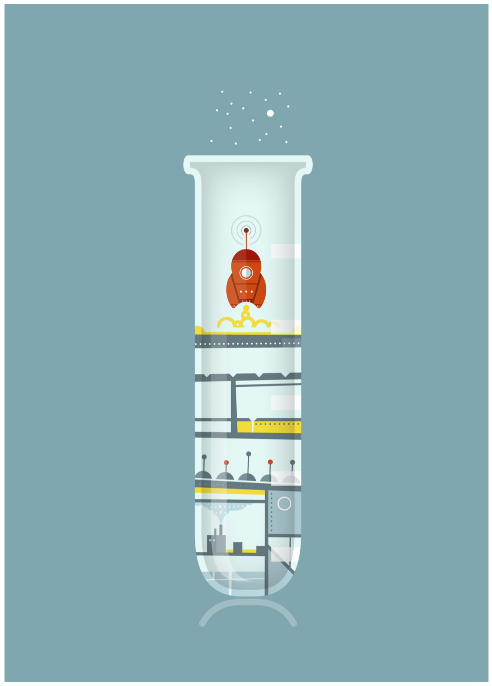

THIS THESIS WAS TYPESET using LaTeX, originally developed by Leslie Lamport and based on Donald Knuth's TeX. The body text is set in 11 point Egenolff-Berner Garamond, a revival of Claude Garamont's humanist typeface. The above illustration, *Science Experiment 02*, was created by Ben Schlitter and released under CC BY-NC-ND 3.0. A template that can be used to format a PhD dissertation with this look & feel has been released under the permissive AGPL license, and can be found online at github.com/asm-products/Dissertate or from its lead author, Jordan Suchow, at suchow@post.harvard.edu.